Supporting Information

A Novel Photoswitchable AIE-Active Supramolecular Photosensitizer with Synergistic Enhancement of ROS-Generation Ability Constructed by A Two-Step Sequential FRET Process

Xueqi Tian [1], Shengke Li [2], Krishnasamy Velmurugan [1], Zhihang Bai [1], Qian Liu [1], Kaiya Wang [1], Minzan Zuo [1] and Xiao-Yu Hu [1]**

[1]College of Materials Science and Technology, Nanjing University of Aeronautics and Astronautics, Nanjing 211106, P. R. China

[2]State Key Laboratory of Quality Research in Chinese Medicine, Institute of Chinese Medical Sciences, University of Macau, Macau 999078, P. R. China

*Corresponding Author: minzanzuo@nuaa.edu.cn; huxy@nuaa.edu.cn

Table of Contents

1. Experimental procedure

General information. All the reagents and solvents were commercially available and used as received unless otherwise specified purification. NMR spectra were recorded on a Bruker AV400 instrument. High-resolution electrospray ionization mass spectra (HR-ESI-MS) were recorded on an Agilent 6540Q-TOF LCMS equipped with an electrospray ionization (ESI) probe operating in the positive-ion mode with direct infusion. UV/vis spectra were recorded on a Shimadzu UV-1700 spectrophotometer. The fluorescence lifetimes were measured by time-correlated single photon counting on a FLS1000 instrument (Edinburg Instruments Ltd., Livingstone, UK). Transmission electron microscope (TEM) investigations were carried out on a FEI Talos F200X instrument. The sample solutions for dynamic light scattering measurement (DLS) were carried out on a Brookhaven BI-9000AT system (Brookhaven Instruments Corporation, USA), using a 200 mW polarized laser source (λ = 514 nm) at a scattering angle of 90°. Zeta-potential measurements were performed at 25 °C on a Brookhaven BI-9000AT system (Brookhaven Instruments Corporation, USA), using the Smoluchowski model for the calculation of the Zeta-potential from the measured electrophoretic mobility. Fluorescence images were taken with a fluorescence microscope (Olympus IX51).

Photochemical conversion yield.[S1] The photochemical conversion yield (ϕ_c) from **SP-G** to **MC-G** can be obtained by UV/vis spectroscopy. According to the literature, the photochemical conversion yield (ϕ_c) was calculated according to equation (1):

$$\Phi_c = \frac{A}{\varepsilon_A L C_0} \qquad \textbf{(1)}$$

A is the absorbance for **MC-G** at 520 nm upon UV irradiation, ε_A is the molar absorption coefficient (ε_A) of **MC-G** at the λ_{max} (520 nm), L is the path length of the sample (1 cm for the present case), and C_0 is the actual molar concentration of spiropyran.

Determination of the singlet oxygen quantum yield.[S2] The singlet oxygen quantum yield Φ_Δ was determined by using 1.3-diphenylisobenzofuran (DPBF) quenching assay. Rose bengal was used as the standard for the determination of ROS quantum yield. The photodegradation of DPBF was determined by the measurement of the absorbance of DPBF at 410 nm. The ROS quantum yield of **MC-G**, **NiB**, ***m*-TPEWP5⊃MC-G**, ***m*-TPEWP5⊃MC-G-NiB** was calculated using equation (2):

$$\emptyset_\Delta = \emptyset_{RB} \times \frac{K_\Delta}{K_{RB}} \qquad \textbf{(2)}$$

Where *K* is the photodegradation rate constant of DPBF, and the Rose Bengal as the reference standard. It was reported that the ROS quantum yield of the reference compound, Rose Bengal (Φ_{RB}), is 0.75 when dissolved in water.

The photodegradation rate constants of DPBF by samples were determined as the time-dependent decrease of the absorbance of DPBF (A) at 410 nm, as denoted by equation (3):

$$K = d(ln(A_0/A_t))/d(t) \quad \textbf{(3)}$$

Where A_o is the absorbance of DPBF before irradiation with visible light, and A_t is the absorbance of DPBF after t s of visible light irradiation.

***In vitro* cytocompatibility and cytotoxicity assay.** CCK-8 kit was used to evaluate the cell viability. HeLa cells (Bairui Biotech. Ltd, Nanjing, China) were seeded in a 6-well plate at 5×10^3 cells per well in 100 μL of dulbecco's modified eagle medium (DMEM) containing 10% fetal bovine serum (FBS, Gibco), 50 U·mL^{-1} penicillin, and 50 U·mL^{-1} streptomycin (Hyclone), and cultured in 5% CO_2 at 37 °C for 24 h. The HeLa cells were treated with different concentrations (0.05, 0.1, 0.2, 0.3 and 0.4 μM) of **MC-G**, ***m*-TPEWP5⊃MC-G**, ***m*-TPEWP5⊃MC-G-NiB**. Cells without any treatments served as the control group. After incubating for 4 h, cells were subjected to alternating UV and visible light irradiation treatments, and incubated for another 24 h. After 24 h, 10% of CCK-8 solution with a culture medium was added to each well to stain the live cells. Then, the cells were placed in an incubator for 3 h (5% CO_2, 37 °C). Finally, analysis of the 6-well plates with a microplate reader (KAYTO, RT-6000) was performed, and the results were then statistically analyzed and plotted. The cytocompatibility and cytotoxicity were expressed as the percentage of the cell viability relative to the blank control.

Flow cytometric analysis.[S3] HeLa cells were seeded into 6-well plates (1×10^5 per well) and incubated in complete DMEM containing 10% FBS at 37 °C under 5% CO_2 for 24 h. Then the cells were incubated with ***m*-TPEWP5⊃MC-G-NiB** nanoparticles (**NP2**) for 4 h. After washing twice with phosphate-buffered sline (PBS), cells were subjected to alternating UV and visible light irradiation treatments, cultured for another 24 h, and digested by trypsinization, centrifuged at 2000 rpm for 5 min, then culture medium was removed and the cells were washed with PBS twice. After removing of the supernatants, the cells were resuspended in binding buffer (500 μL). Annexin V-FITC (5 μL) was added to the cell suspensions, after incubation in the dark for 15 mins, cells were stained by the Annexin V-FITC apoptosis detection kit (Bairui Biotech, Nanjing, China), and analyzed through flow cytometry.

Cell imaging. HeLa cells were seeded at a density of 1×10^4 cells per well in 6-well glass-bottomed plates and incubated in complete DMEM containing 10% fetal bovine serum in the 37 °C incubator containing 5% CO_2 for 24 h. The cells were incubated with **MC-G**, ***m*-TPEWP5⊃MC-G**, ***m*-TPEWP5⊃MC-G-NiB**, respectively, for additional 4 h. After washing twice with PBS, the cells were imaged by fluorescence microscope (OLYMPUS IX51).

Antibacterial experiments.[S4] The bacteria were incubated with ***m*-TPEWP5⊃MC-G-NiB** nanoparticles (**NP2**, 10 μM) at 37 ℃ for 10 min, and the bacteria were irradiated upon various photoswitching cycles (UV-365 nm, 32 mW cm^{-2} for 1 min; visible light, >500 nm, 20 mW cm^{-2} for 2 mins) or under dark. The diluted bacterial sample (100 μL) was spread on a solid LB agar plate, and the number of colonies formed after 24 h of incubation at 37 °C were counted. The inhibition ratio was determined by equation (4) :

$$CFU\ Ratio = \frac{C}{C_0} \times 100\% \qquad \textbf{(4)}$$

C is the CFU of the experimental group treated with **NP2** under different light irradiation, and C_0 is the CFU of the control group without any treatment.

The antibacterial inhibition ratio was determined by equation (5):

$$IR = (C_0 - C)/C_0 \times 100\% \qquad \textbf{(5)}$$

C is the CFU of the experimental group treated with **NP2** in the dark or under light irradiation, and C_0 is the CFU of the control group without any treatment.

2. Synthesis of host molecule *m*-TPEWP5 and guest molecule SP-G

Synthesis of host molecule *m*-TPEWP5[S5]

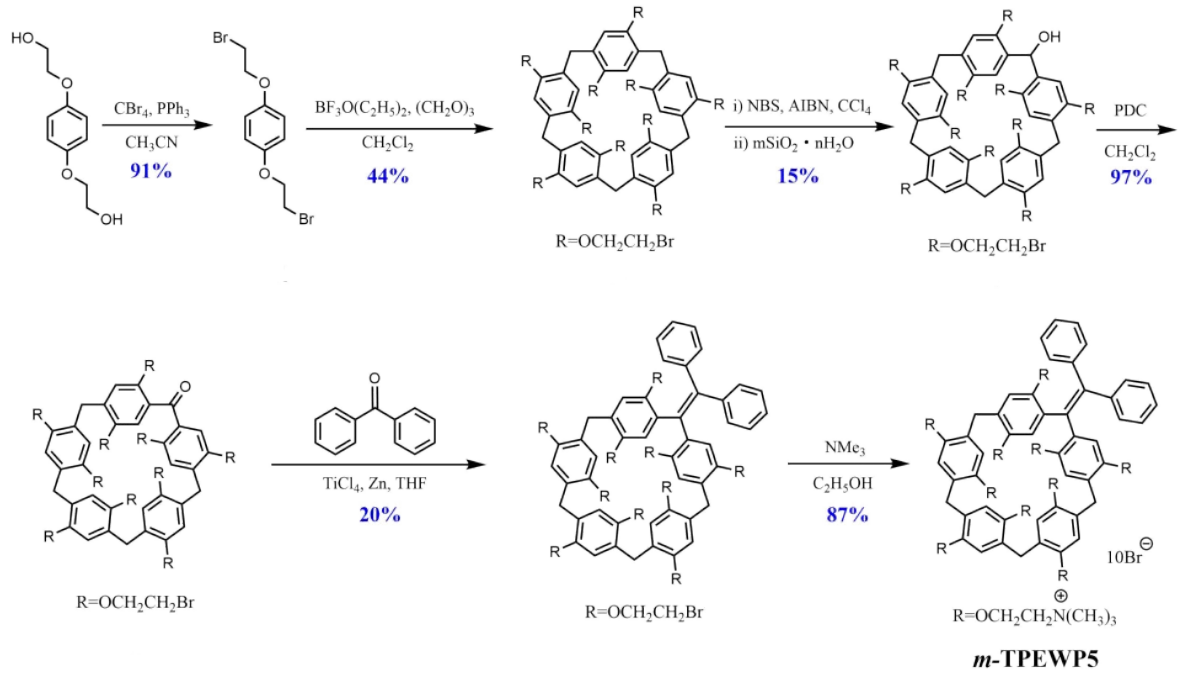

Scheme S1. Synthesis route of host molecule ***m*-TPEWP5**.

Synthesis of guest molecule SP-G[S6]

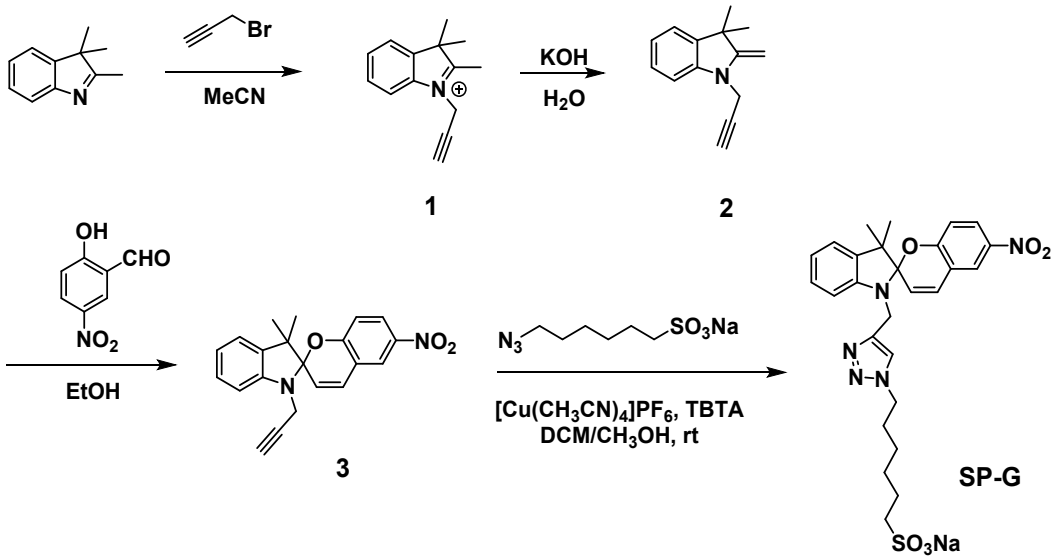

Scheme S2. Synthesis route of guest molecule **SP-G**.

Synthesis of compound 1

A solution of 2,3,3-trimethylindolenine (3.02 g, 18.73 mmol) in acetonitrile (60 mL) was reflux under N_2. Then propargyl bromide (3.30 mL, 27.74 mmol) was added to the solution and refluxed overnight. Acetonitrile was removed by vacuum system, and a brown oil (5.45 g) was obtained as a crude product. The mixture was directly used for the next step.

Synthesis of compound 2

A solution of compound **1** (3.6 g, 18.16 mmol) in aqueous KOH (1.6 M, 50 mL) was stirred at room temperature under N_2 for 30 min. The solution was extracted with ethyl acetate (3 × 50 mL). The organic phase was washed with water (3 × 50 mL) and dried over with Na_2SO_4, and distilled off under reduced pressure. The residue was purified on silica gel using column chromatography with hexane to give the desired product as a brown oil and directly used for the next step. ^{1}H NMR (400 MHz, $CDCl_3$, 298 K) δ (ppm): 7.17-7.10 (m, 2H), 6.82 (s, 1H), 6.65 (d, J = 7.8 Hz, 1H), 4.26 (s, 2H), 4.01 (d, J = 12.9 Hz, 2H), 2.14 (s, 1H), 1.36 (s, 6H).

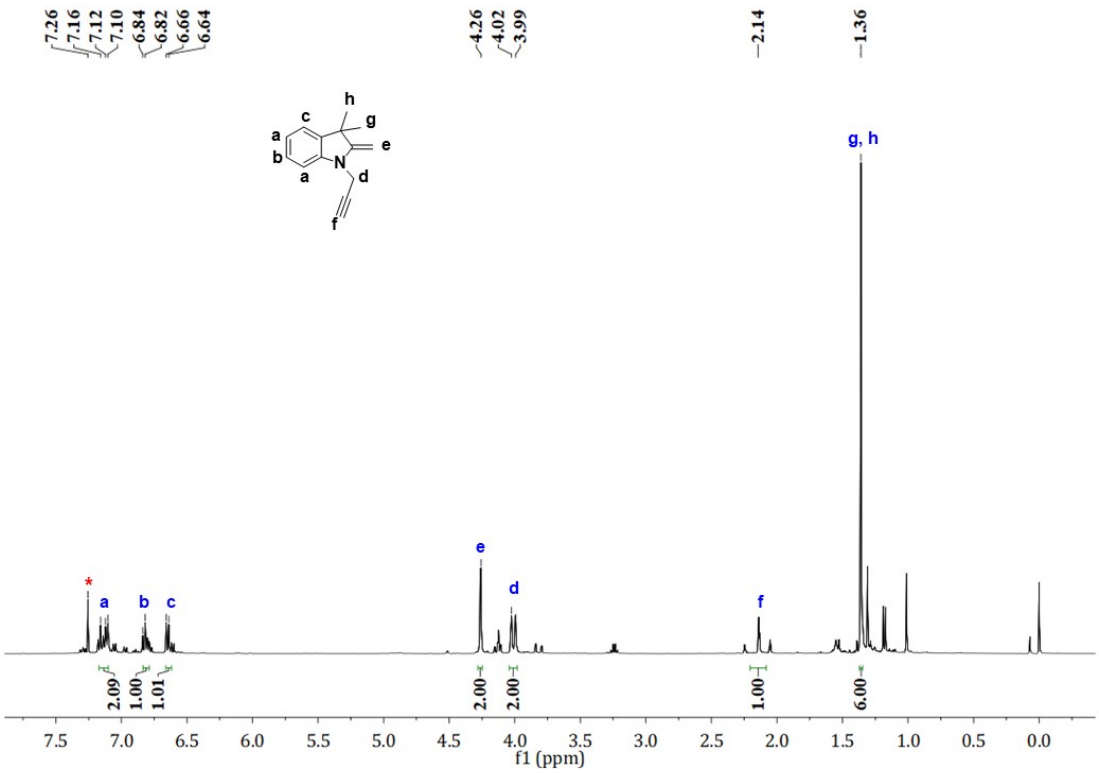

Fig. S1 ^{1}H NMR spectrum (400 MHz, $CDCl_3$, 298 K) of compound **2**.

Synthesis of compound 3

A solution of 2-hydroxy-5-nitrobenzaldehyde (0.79 g, 4.0 mmol) was dissolved in ethanol under reflux. Compound **2** (0.75 g, 4.5 mmol) was added to the above solution and refluxed under N_2 for 3 h. The mixture was concentrated under vacuum and the residue was purified on silica gel column chromatography with a mixed elution system of hexane/ethyl acetate (Hex/EtOAc = 50:1, *v/v*) to give the desired product as a brown solid (0.69 g, 1.99 mmol, 50% yield). ^{1}H NMR (400 MHz, $CDCl_3$, 298 K) δ (ppm): 8.06-8.00 (m, 2H), 7.22 (dd, J = 7.7, 1.1 Hz, 1H), 7.12 (dd, J = 7.3, 0.6 Hz, 1H), 6.99-6.92 (m, 2H), 6.82 (d, J = 7.8 Hz, 1H), 6.75 (d, J = 9.9 Hz, 1H), 5.89 (d, J = 10.3 Hz, 1H), 4.07-3.83 (m, 2H), 2.09 (s, 1H), 1.30 (s, 3H), 1.20 (s, 3H).

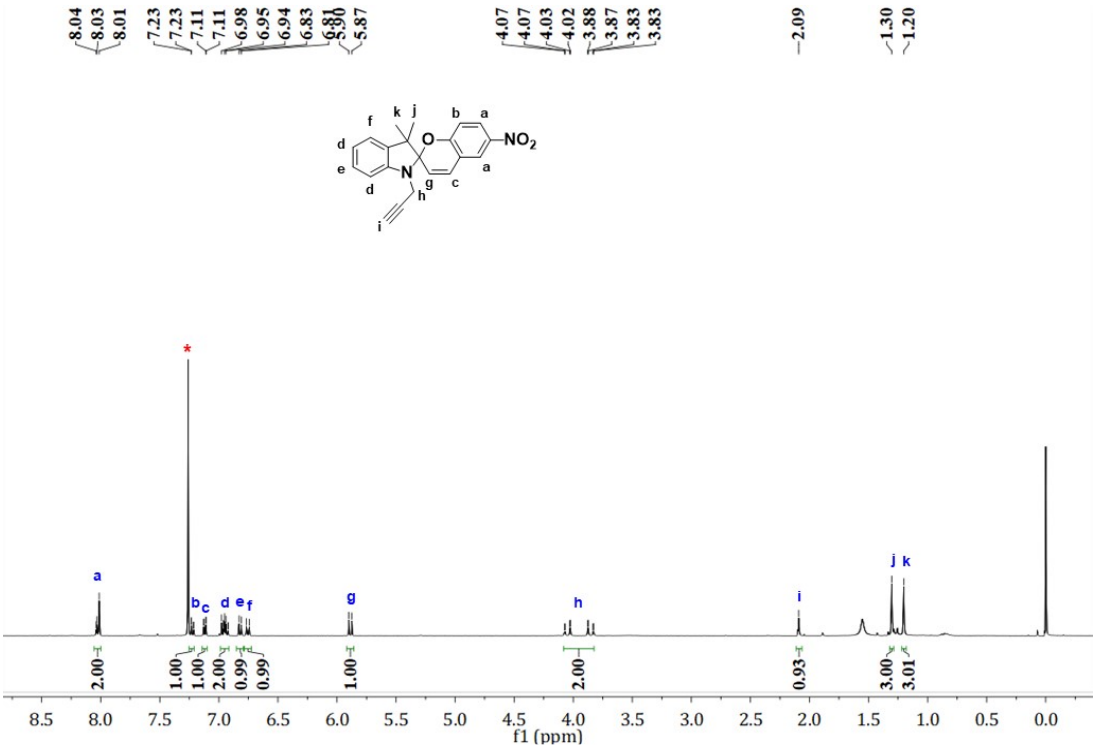

Fig. S2 ^{1}H NMR spectrum (400 MHz, $CDCl_3$, 298 K) of compound **3**.

Synthesis of compound SP-G

Compound **3** (0.15 g, 0.43 mmol), N_3-SO_3Na (0.13 g, 0.56 mmol)[S5] and TBTA (0.023 g, 0.043 mmol) were dissolved in dry mixed solvent DCM/MeOH (10 mL, 1:1, *v/v*) at room temperature, and continuously stirred for 10 min. Then, $[Cu(CH_3CN)_4]PF_6$ (0.02 g, 0.043 mmol) was added. The solution was stirred at room temperature for 24 h. The solvent was removed, and the residue was dissolved in MeOH and precipitated with ethyl ether. The obtained light-pink precipitate was washed with ethyl ether to afford SP-G as a pink powder (0.18 g, 0.31 mmol, 72% yield). ^{1}H NMR (400 MHz, DMSO-d_6, 298 K) δ (ppm): 8.21 (d, J = 2.5 Hz, 1H), 8.00 (dd, J = 8.9, 2.5 Hz, 1H), 7.92 (s, 1H), 7.24 (d, J = 10.4 Hz, 1H), 7.12 (dd, J = 16.3, 7.3 Hz, 2H), 6.86-6.77 (m, 2H), 6.58 (d, J = 7.8 Hz, 1H), 6.07 (d, J = 10.3 Hz, 1H), 4.47 (d, J = 15.8 Hz, 1H), 4.32 (d, J = 15.2 Hz, 1H), 4.25 (t, J = 7.0 Hz, 2H), 2.38-2.33 (m, 2H), 1.75-1.67 (m, 2H), 1.54-1.49 (m, 2H), 1.31-1.13 (m, 10H). ^{13}C NMR (100 MHz, DMSO-d_6, 298 K): δ (ppm): 159.53, 146.72, 140.99, 136.08, 129.03, 128.01, 126.15, 123.31, 122.10, 119.86, 119.29, 115.94, 107.53, 106.59, 52.85, 51.80, 49.66, 30.10, 28.17,

26.21, 25.46, 20.01. HR-ESI-MS: *m/z* $[M + H]^+$ calcd for $[C_{27}H_{31}N_5NaO_6S]^+$ 576.1893, found 576.1944.

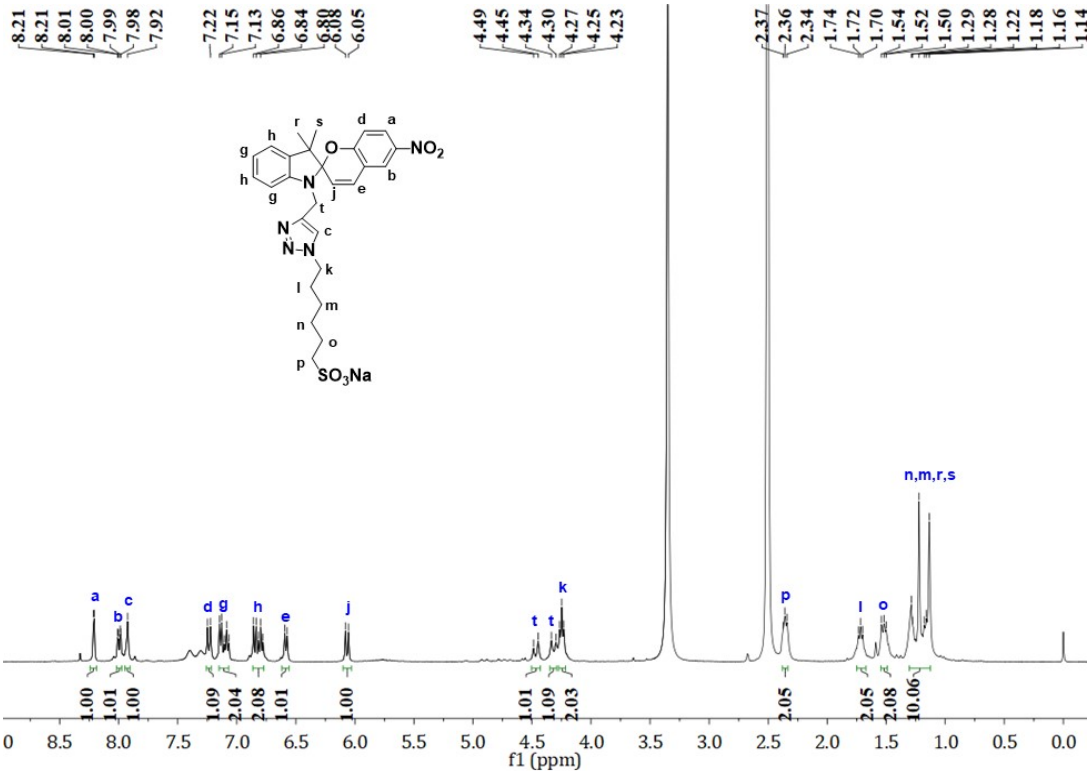

Fig. S3 ^{1}H NMR spectrum (400 MHz, DMSO-d_6, 298 K) of compound **SP-G**.

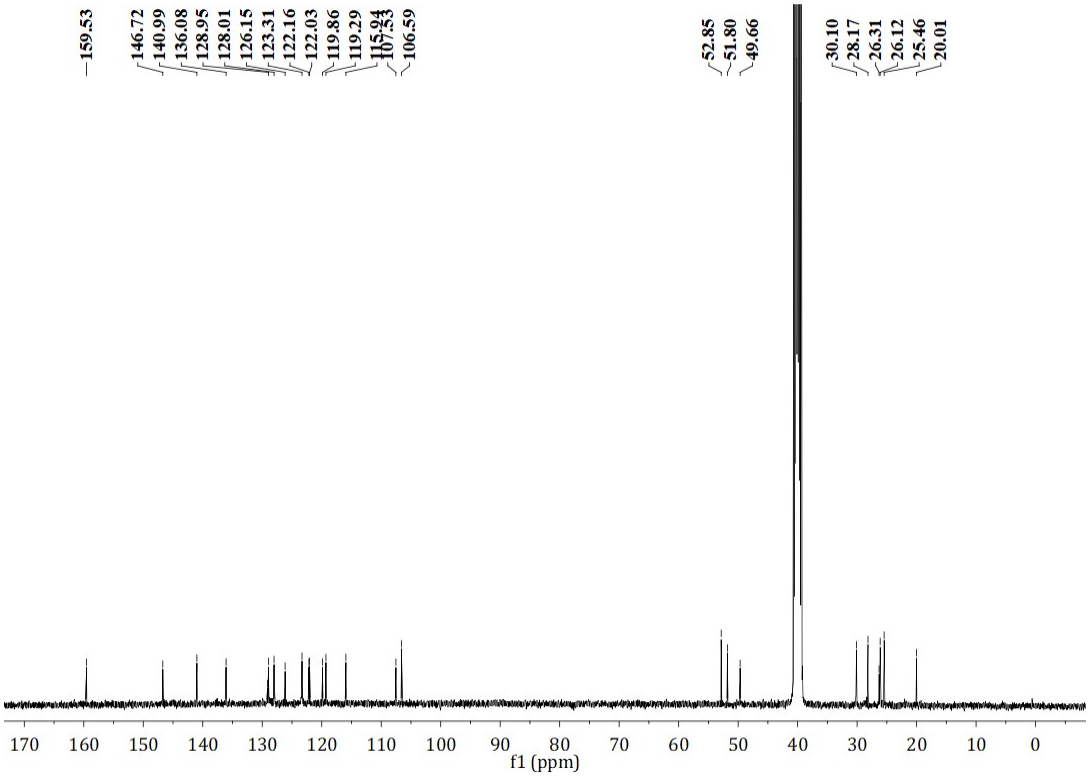

Fig. S4 ^{13}C NMR spectrum (100 MHz, DMSO-d_6, 298 K) of compound **SP-G**.

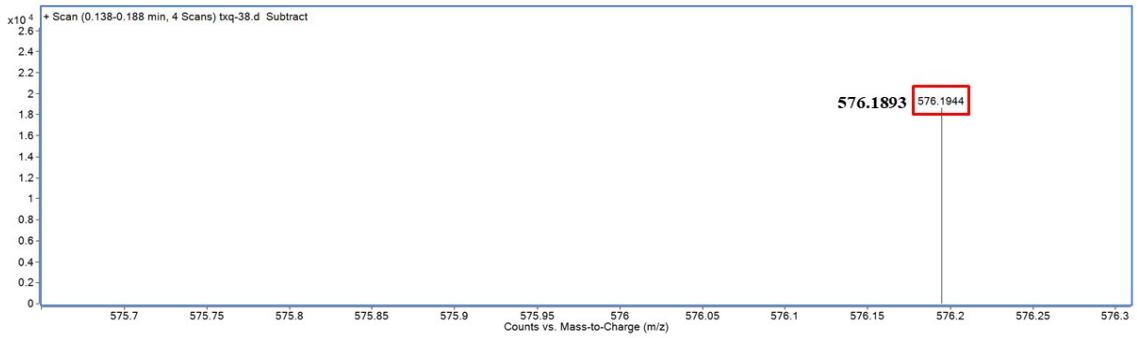

Fig. S5 HR-ESI-MS spectra of compound **SP-G**.

3. Photoswitching study of SP-G

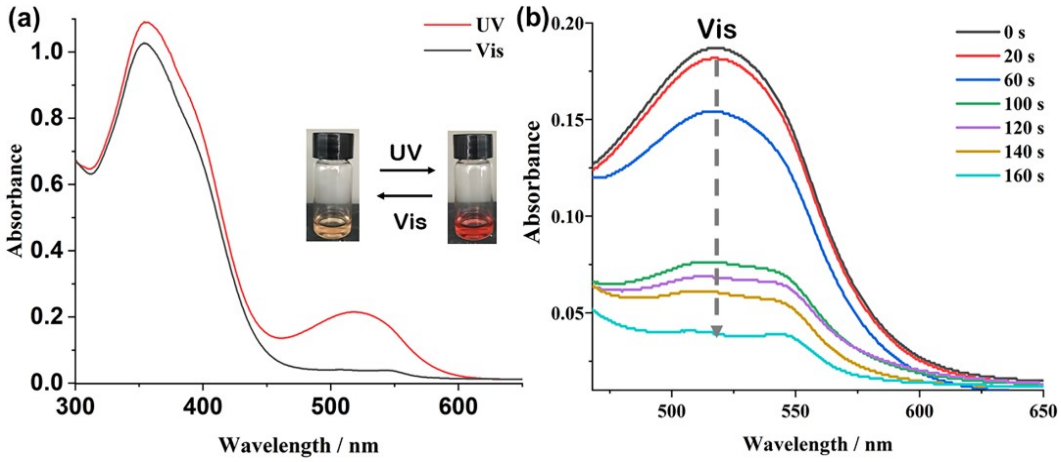

Fig. S6 (a) Absorption spectra (inset: images observed by naked-eyes) of reversible photoswitching of **SP-G** upon irradiating by UV-light (365 nm, red line) and visible-light (>500 nm, 20 mW cm^{-2}, black line), (b) Absorption spectra of **MC-G** upon irradiating by visible-light (>500 nm, 20 mW cm^{-2}) for different time periods. [**SP-G**] = [**MC-G**] = 0.1 mM.

4. Job's plot for *m*-TPEWP5 and SP-G

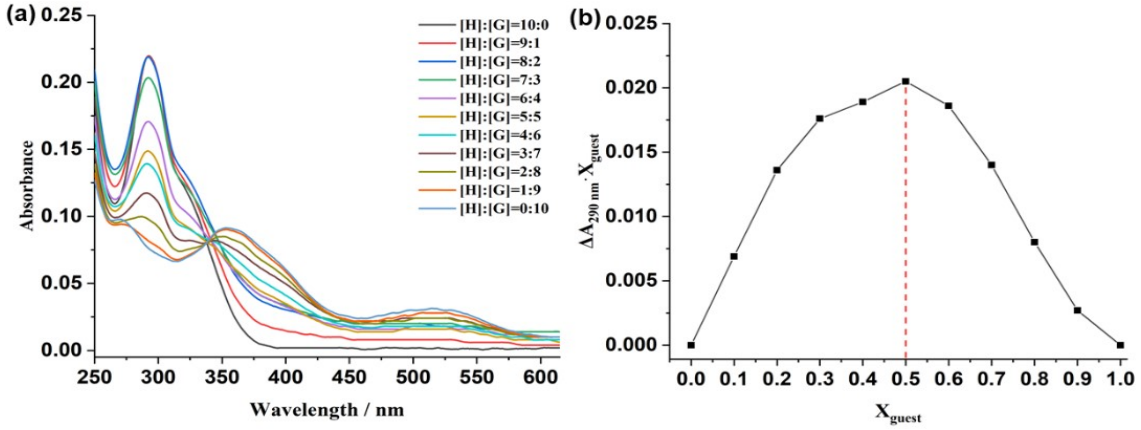

Fig. S7 (a) UV-vis absorbance of the mixture of ***m*-TPEWP5** (H) and **SP-G** (G) in water at different molar ratio while [***m*-TPEWP5**] + [**SP-G**] = 2×10^{-5} M, (b) Job's Plot showing 1:1 stoichiometry of the complex between ***m*-TPEWP5** and **SP-G** by plotting the absorbance differences at 290 nm (a characteristic absorption peak of ***m*-TPEWP5**) against the mole fraction of **SP-G**.

5. Investigation of the binding constant between m-TPEWP5 and SP-G

To determine the association constant between ***m*-TPEWP5** and **SP-G**, UV-vis measurements were carried out in aqueous solution, which had a constant concentration of ***m*-TPEWP5** (0.02 mM) and varying concentrations of **SP-G**. By a non-linear curve-fitting method, the association constant between the **SP-G** and ***m*-TPEWP5** was calculated. The non-linear curve-fitting was based on the following equation (6):

$$\Delta A = (\Delta A_\infty/[H]_0)\ (0.5[G]_0 + 0.5([H]_0+1/K_a) - (0.5([G]_0^2 + (2[G]_0(1/K_a - [H]_0)) + (1/K_a+[H]_0)^2)^{0.5})) \quad \textbf{(6)}$$

Where ΔA is the UV-vis absorption changes at 290 nm at $[H]_0$, ΔA_∞ is the UV-vis absorption changes at 290 nm when ***m*-TPEWP5** is completely complexed, $[H]_0$ is the fixed initial concentration of the host (***m*-TPEWP5**), and $[G]_0$ is the varying concentrations of the guest (**SP-G**). By non-linear fitting the spectrum data with the above equation, the binding constant K_a was determined to be $(2.30 \pm 0.34) \times 10^4\ M^{-1}$.

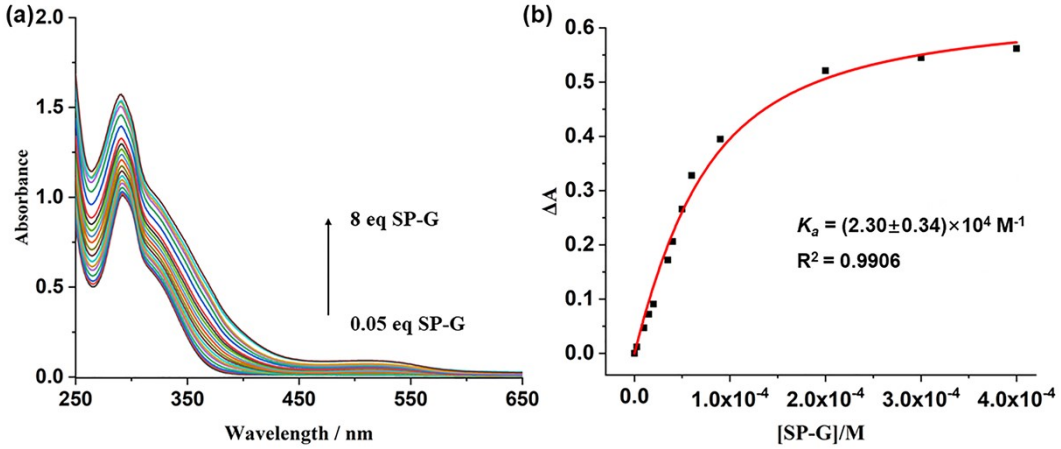

Fig. S8 (a) The UV-vis absorption changes of ***m*-TPEWP5** upon the addition of **SP-G**, (b) The red solid line was obtained from the non-linear curve-fitting. The association constant (K_a) of ***m*-TPEWP5** and **SP-G** was estimated to be $(2.30 \pm 0.34) \times 10^4\ M^{-1}$.

6. Determinations of the best molar ratio between *m*-TPEWP5 and MC-G for fabricating nanoaggregates

The best molar ratio between ***m*-TPEWP5** and **MC-G** was determined by measuring the fluorescence intensity at 465 nm with different molar fractions of **MC-G** in aqueous solution. As the **MC-G** concentration was gradually increased with respect to ***m*-TPEWP5** (1 equiv.), the fluorescence intensity at 465 nm decreased to a minimum at the molar ratio of ***m*-TPEWP5:MC-G** (1:4) and then increased reversely when further increasing the molar ratio of **MC-G**. The above results indicated that the best molar ratio between ***m*-TPEWP5** and **MC-G** for constructing supramolecular nanoaggregates was 1:4.

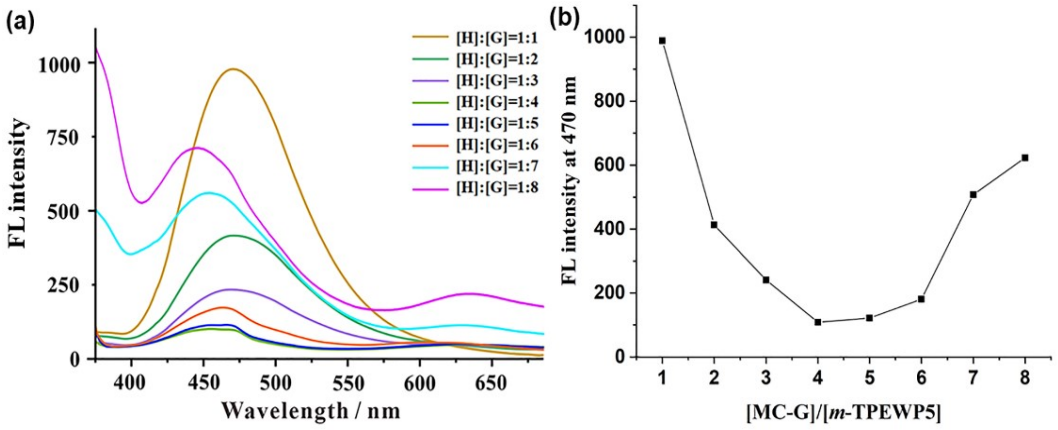

Fig. S9 (a) Fluorescence emission spectra of with a constant concentration of ***m*-TPEWP5** (**H**) in aqueous solutions by increasing the concentration of **MC-G** (**G**, 1–8 equiv.) at 25 °C, (b) Dependence of the relative fluorescence intensity at 470 nm on the **MC-G** concentration with a fixed concentration of ***m*-TPEWP5** at 25 °C. [***m*-TPEWP5**] = 0.1 mM.

7. Energy transfer efficiency measurement

Energy-transfer efficiency (Φ_{ET}), the fraction of the absorbed energy that is transferred to the acceptor, is experimentally measured as a ratio of the fluorescence intensities of the donor in the absence and presence of the acceptor (I_D and I_{DA}) by the equation (7) [S7]:

$$\emptyset_{ET} = 1 - \frac{I_{DA}}{I_D} \qquad (7)$$

The energy-transfer efficiency (ϕ_{ET}) was calculated in water, measured under the condition of [***m*-TPEWP5**] = 20 μM, [**MC-G**] = 80 μM, [**NiB**] = 2 μM, λ_{ex} = 365 nm.

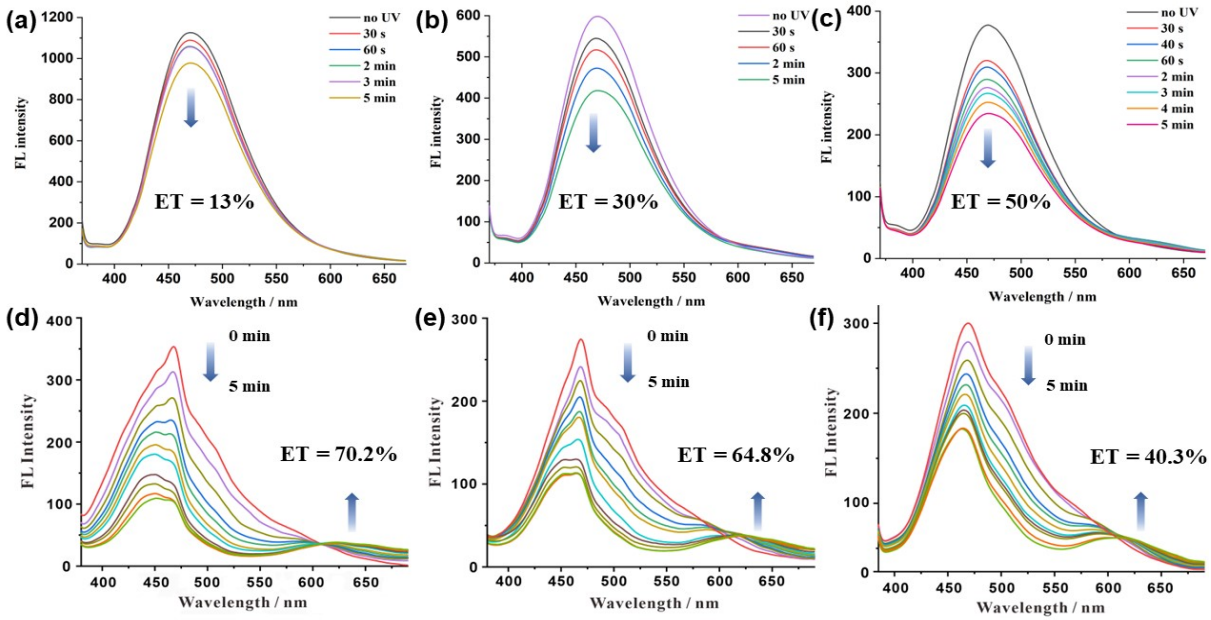

Fig. S10 Determination of the energy-transfer efficiency (ϕ_{ET}) between **MC-G** and ***m*-TPEWP5** with different [***m*-TPEWP5**]/[**MC-G**] ratios: (a) 1:1, (b) 2:1, (c) 3:1, (d) 4:1, (e) 5:1, (f) 6:1.

8. TEM images of *m*-TPEWP5⊃SP-G and *m*-TPEWP5⊃SP-G-NiB nanoparticles

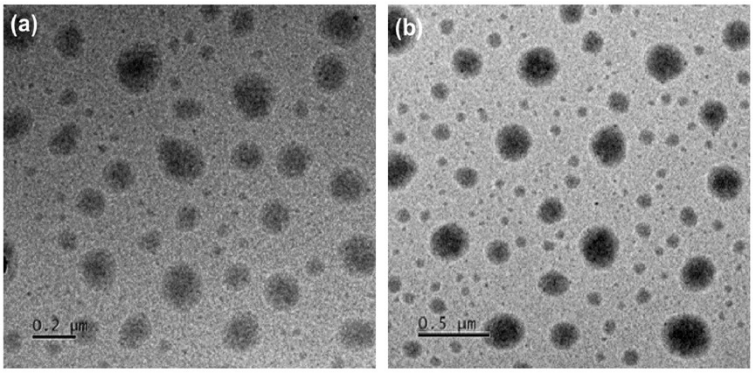

Fig. S11 TEM images of (a) ***m*-TPEWP5⊃SP-G** nanoparticles (scale bar = 0.2 μm), (b) ***m*-TPEWP5⊃SP-G-NiB** nanoparticles (scale bar = 0.5 μm) under three alternating cycles (UV light, 365 nm, 32 mW cm^{-2}); visible light, >500 nm, 20 mW cm^{-2}). [***m*-TPEWP5**] = 20 μM, [**SP-G**] = 80 μM, [**NiB**] = 2 μM.

9. Zeta-potential and DLS measurements

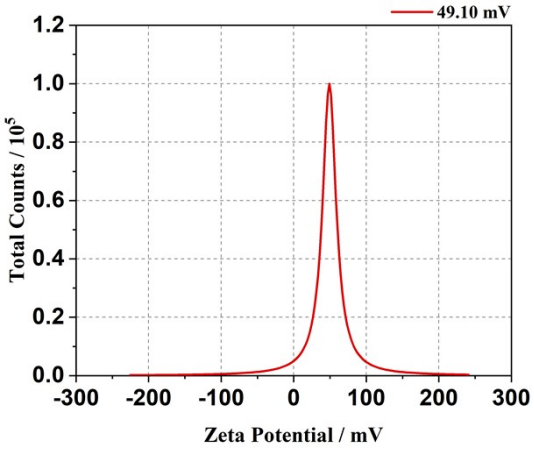

Fig. S12 Zeta-potential of ***m*-TPEWP5⊃MC-G-NiB** nanoparticle. [***m*-TPEWP5**] = 20 μM, [**MC-G**] = 80 μM, [**NiB**] = 2 μM.

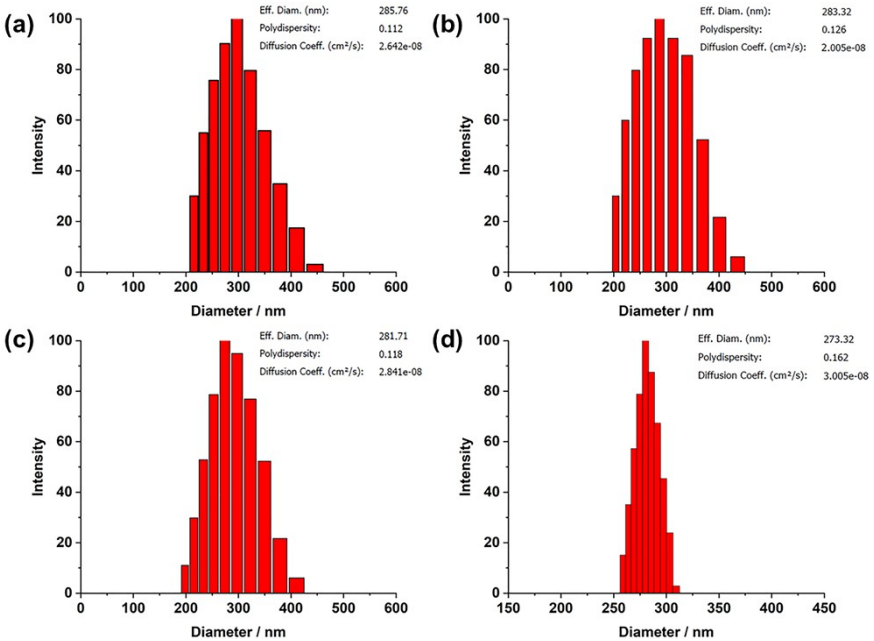

Fig. S13 DLS data of ***m*-TPEWP5⊃MC-G-NiB** nanoparticle after standing for 1−4 weeks.

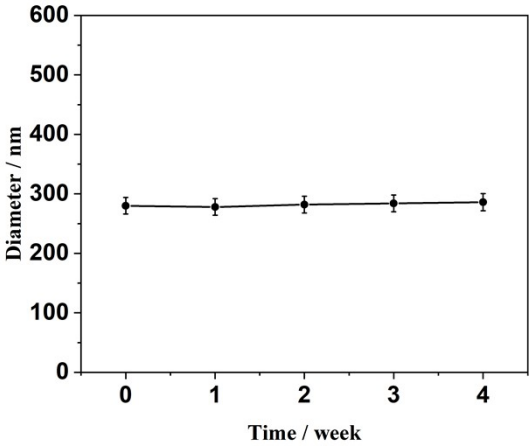

Fig. S14 Time-dependent size changes of ***m*-TPEWP5⊃MC-G-NiB** nanoparticle.

10. FRET process under visible irradiation

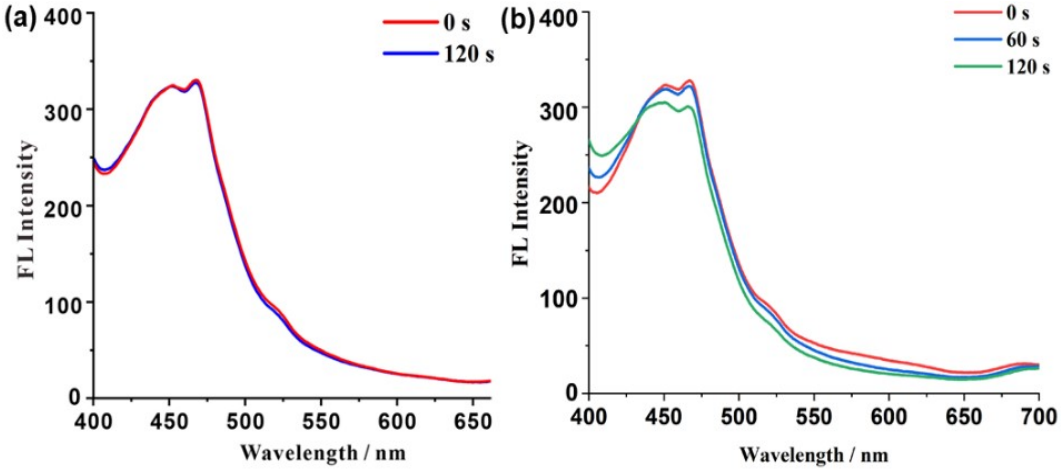

Fig. S15 Upon continuous irradiation with visible light (>500 nm, 20 mW cm^{-2}): (a) fluorescence spectral changes of ***m*-TPEWP5⊃SP-G** nanoparticles, (b) fluorescence spectral changes of ***m*-TPEWP5⊃SP-G-NiB** nanoparticles. [***m*-TPEWP5**] = 20 μM, [**SP-G**] = 80 μM, [**NiB**] = 2 μM.

11. Fluorescence quantum yield

The fluorescence quantum yields were determined using equation (8)[S7]:

$$\varphi_i = \varphi_s \cdot \frac{n^2}{n_s^2} \cdot \frac{I_i}{I_s} \cdot \frac{1 - 10^{-A_S(\lambda_{exc})}}{1 - 10^{-A_i(\lambda_{exc})}} \qquad \textbf{(8)}$$

Where φ is the fluorescence quantum yield, A is the absorbance at the excitation wavelength, I is the area under the fluorescence spectra, and n is the refractive index of the solvent in which the sample was collected. The subscripts "i" and "s" refer to the sample of interest and the standard, respectively.

12. Fluorescence lifetime measurements

Table S1. Multiexponential fit parameters for the decay of photoluminescence lifetimes at 365 nm ($\tau = \tau_1 \times Rel_1\% + \tau_2 \times Rel_2\%$) and quantum yields of ***m*-TPEWP5**, ***m*-TPEWP5⊃MC-G** nanoparticles and ***m*-TPEWP5⊃MC-G-NiB** nanoparticles.

Samples	τ_1/ns	RW_1[%]	τ_2/ns	RW_2[%]	τ_{av}/ns	χ^2	Quantum Yield (%)
m-TPEWP5	3.09	49.97	23.29	50.03	13.1	1.15	3.24
m-TPEWP5⊃MC-G	3.16	48.29	19.05	51.71	11.37	1.17	14.43
m-TPEWP5⊃MC-G-NiB	2.53	50.28	13.48	49.72	7.97	1.19	22.06

13. Absorbance decay of ABDA in the presence of *m*-TPEWP5⊃MC-G-NiB, *m*-TPEWP5⊃MC-G, MC-G, NiB, and RB

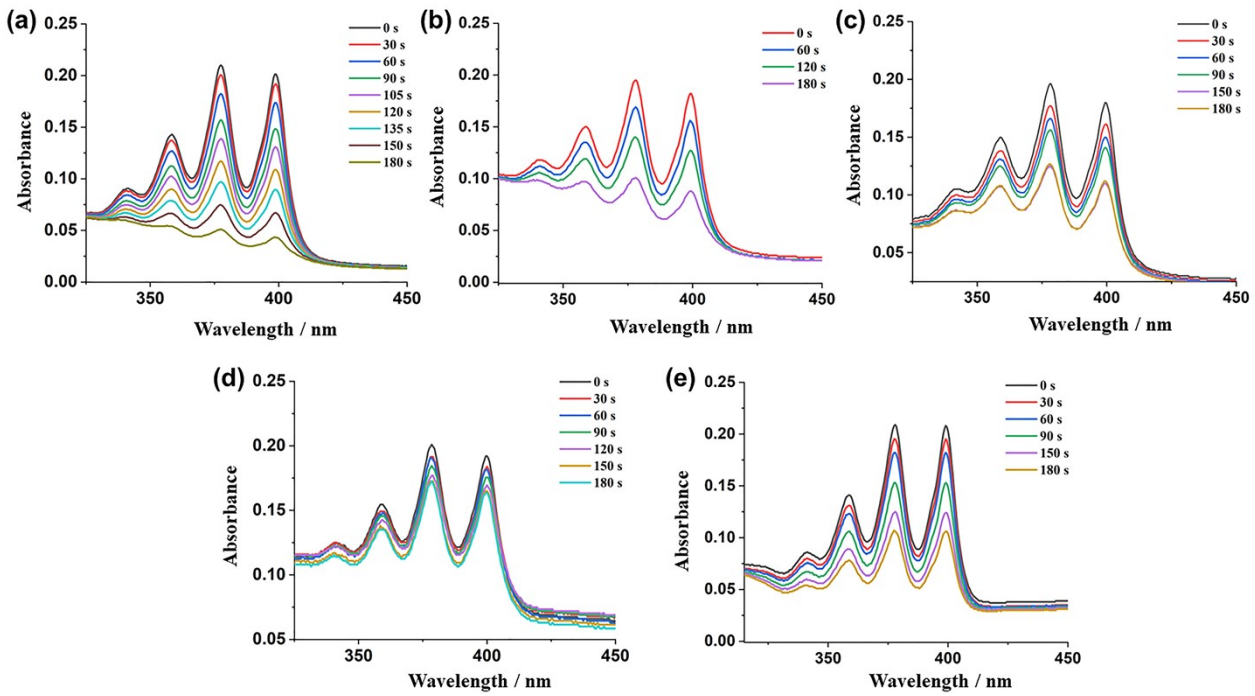

Fig. S16 Absorption spectra of ABDA in the presence of (a) ***m*-TPEWP5⊃MC-G-NiB** (**NP2**), (b) ***m*-TPEWP5⊃MC-G** (**NP1**), (c) **MC-G**, (d) **NiB**, (e) Rose Bengal (**RB**) under white light irradiation (>500 nm, 20 mW cm^{-2}). [***m*-TPEWP5⊃MC-G-NiB**] = [***m*-TPEWP5⊃MC-G**] = [**MC-G**] = [**NiB**] = [**RB**] = 15 μM, [ABDA] = 0.20 mM.

14. Determination of singlet oxygen quantum yield

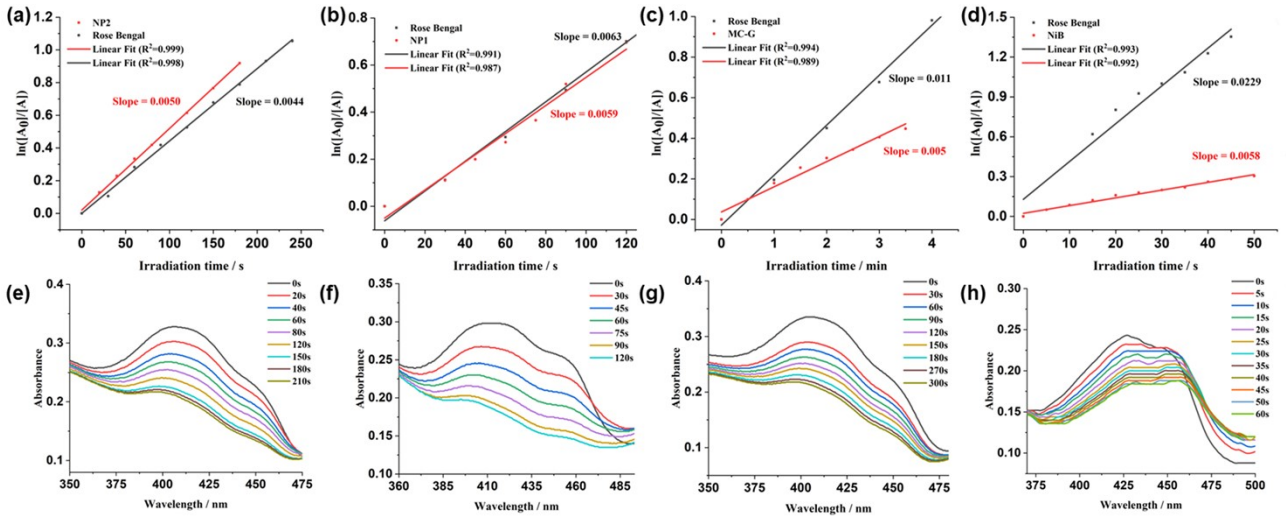

Fig. S17 The time dependence of ln([A_0]/[A]) under visible light irradiation: (a) ***m*-TPEWP5⊃MC-G-NiB (NP2)**, (b) ***m*-TPEWP5⊃MC-G (NP1)**, (c) **MC-G**, (d) **NiB**, respectively. (A_0 is the absorbance of DPBF before irradiation with visible light, and A_t is the absorbance of DPBF after irradiation by visible light for *t* s). The absorption spectra of DPBF in the mixture with (e) ***m*-TPEWP5⊃MC-G-NiB (NP2)**, (f) ***m*-TPEWP5⊃MC-G (NP1)**, (g) **MC-G** (h) **NiB** at different irradiation times under visible light irradiation.

15. Fluorescence images of *m*-TPEWP5⊃MC-G and MC-G

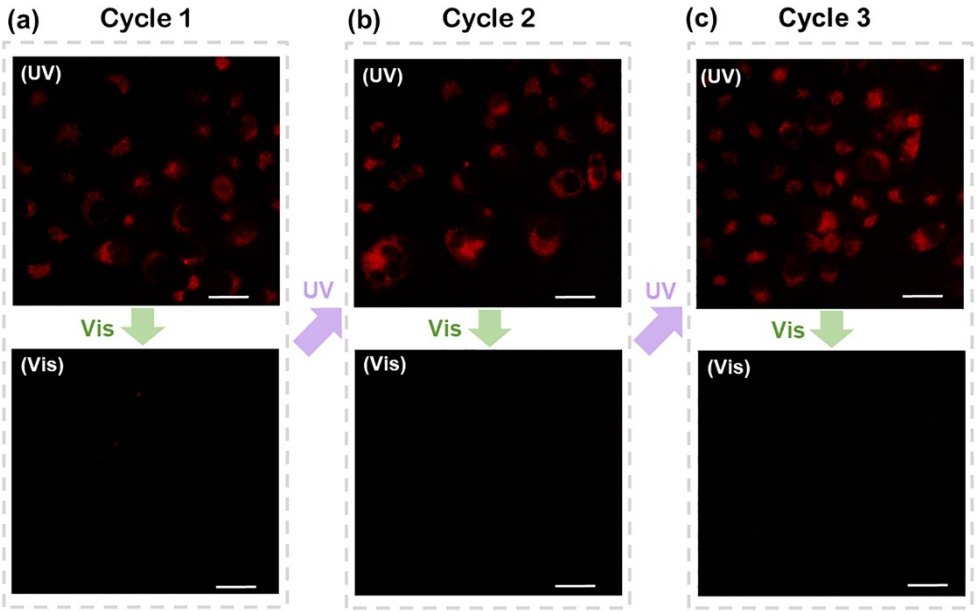

Fig. S18 Fluorescence images of ***m*-TPEWP5⊃MC-G (NP1)** nanoparticles (8 μM) against HeLa cells under alternating UV-light (365 nm, 32 mW cm^{-2}) and visible light (>500 nm, 20 mW cm^{-2}) treatment cycles: (a) cycle 1 (b) cycle 2 (c) cycle 3, respectively. scale bar = 50 μm.

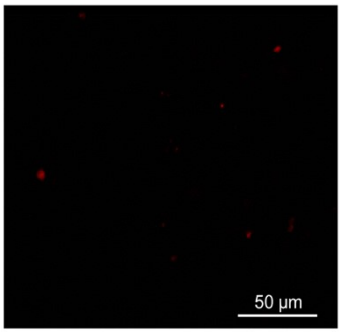

Fig. S19 Fluorescence image of **MC-G** against HeLa cells under UV-light irradiation (365 nm, 32 mW cm^{-2}, 1 min). [**MC-G**] = 8 μM.

16. Reactive oxygen species (ROS) assay

The ROS generation efficacy at cellular level upon light irradiation was examined by using singlet oxygen sensor (SOSG). SOSG is non-emissive, while the oxidation by singlet oxygen will turn on its emission at a wavelength of about 530 nm. HeLa cells were incubated with ***m*-TPEWP5⊃MC-G** nanoparticles (**NP1**) at 37 °C for 4 h in the dark. Then, SOSG was added into the cells, and the final concentration of SOSG was 10 μM. After 30 min incubation, cells were washed twice with PBS and then exposed to light irradiation at the power density of 20 mW cm^{-2}. After light irradiation, the fluorescence images of treated cells were obtained using a fluorescence microscope (OLYMPUS IX51). The SOSG was excited at 504 nm and the emission intensity of the SOSG solution at 530 nm was recorded.[S8]

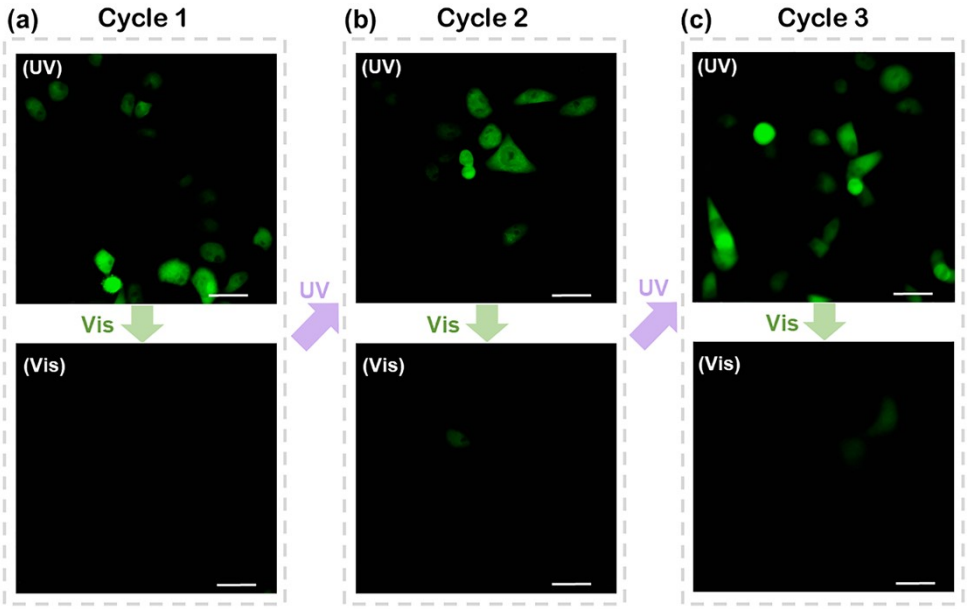

Fig. S20 Oxidized SOSG fluorescence images of ***m*-TPEWP5⊃MC-G** (**NP1**) nanoparticles (8 μM) against HeLa cells under alternating UV-light (365 nm, 32 mW cm^{-2}) and visible light (>500 nm, 20 mW cm^{-2}) treatment cycles: (a) cycle 1, (b) cycle 2, and (c) cycle 3, respectively. scale bar = 50 μm.

In the presence of ROS, 2,7-dichlorodihydrofluorescein diacetate (DCFH-DA) can be converted to DCFH, which is then further transformed into a highly fluorescent DCF. HeLa cells were incubated

with ***m*-TPEWP5⊃MC-G-NiB** nanoparticles (**NP2**) at 37 °C for 4 h in the dark. Then, DCFH-DA was added into the cells, and the final concentration of DCFH was 10 μM. After 30 min incubation, cells were washed three times with PBS and then exposed to light irradiation at the power density of 20 mW cm^{-2}. The excitation wavelength was 488 nm, while the emission intensity of the DCF solution at 500–530 nm was recorded.

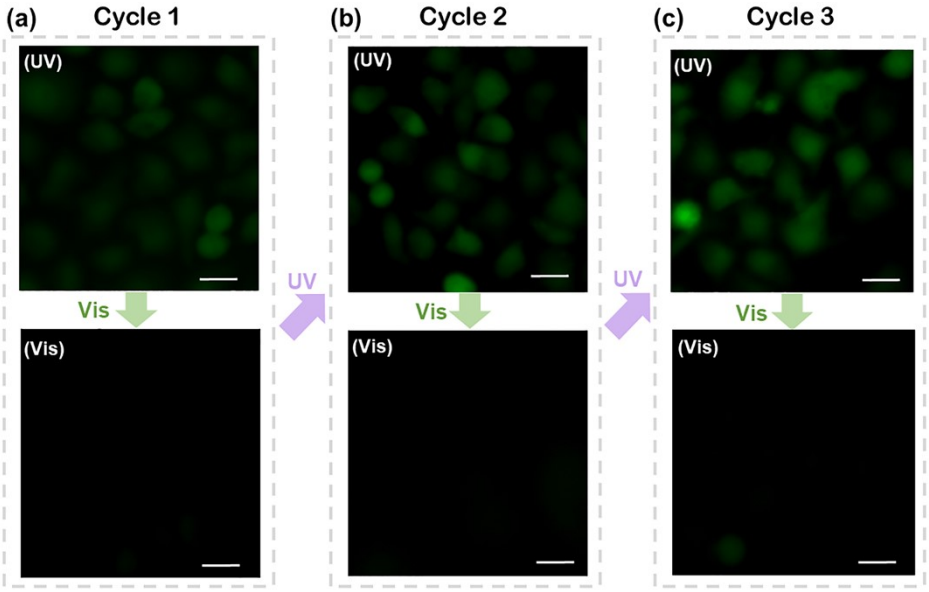

Fig. S21 Oxidized DCF fluorescence images of ***m*-TPEWP5⊃MC-G-NiB** (**NP2**) nanoparticles (8 μM) against HeLa cells under alternating UV-light (365 nm, 32 mW cm^{-2}) and visible light (>500 nm, 20 mW cm^{-2}) treatment cycles: (a) cycle 1, (b) cycle 2, and (c) cycle 3, respectively. scale bar = 50 μm.

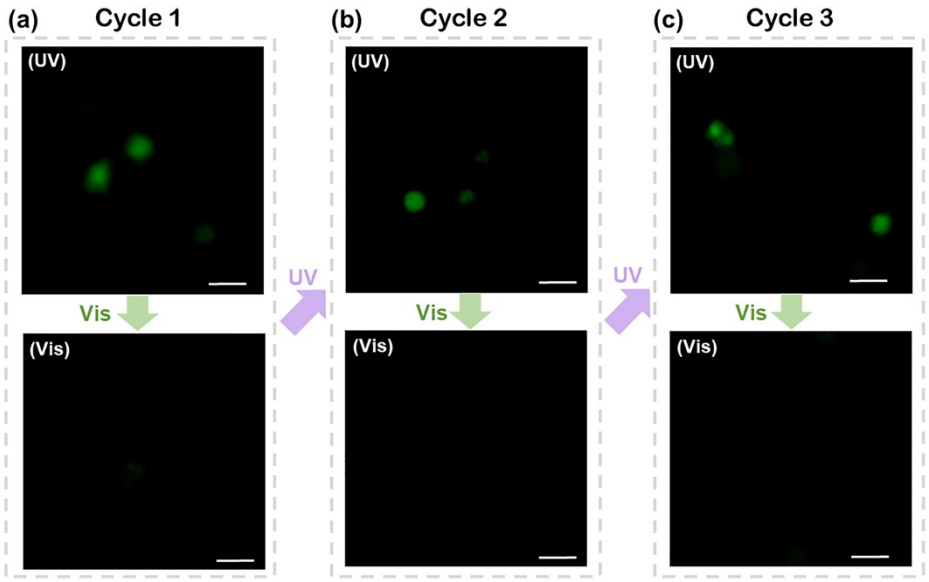

Fig. S22 Oxidized DCF fluorescence images of ***m*-TPEWP5⊃MC-G** (**NP1**) nanoparticles (8 μM) against HeLa cells under alternating UV-light (365 nm, 32 mW cm^{-2}) and visible light (>500 nm, 20 mW cm^{-2}) treatment cycles: (a) cycle 1, (b) cycle 2, and (c) cycle 3, respectively. scale bar = 50 μm.

17. *In vitro* cytotoxicity of MC-G

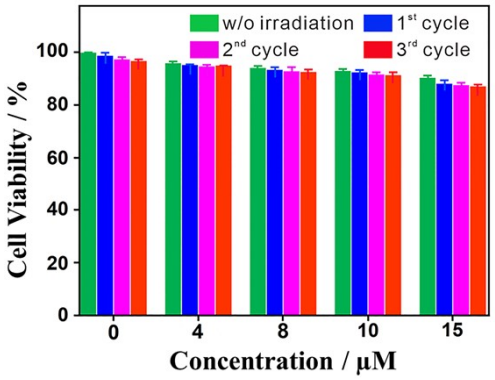

Fig. S23 Cell viability revealed by CCK-8 assays with different concentrations of **MC-G** against HeLa cells after incubation for 24 h under different alternative cycles (UV light, 365 nm, 32 mW cm^{-2}; visible light, >500 nm, 20 mW cm^{-2}).

18. Cell apoptosis analysis by flow cytometry

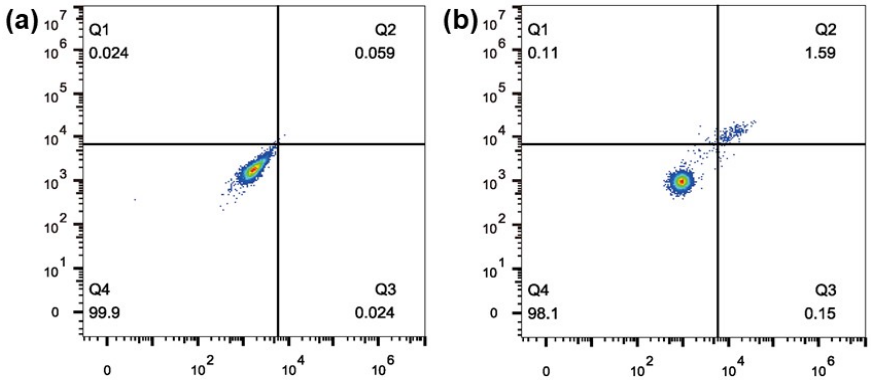

Fig. S24 Flow cytometric analysis of HeLa cells treated with (a) PBS, (b) ***m*-TPEWP5⊃MC-G-NiB** (**NP2**) nanoparticles (10 μM) in dark after incubation for 24 h.

19. Zeta-potential measurements of *E. coli*

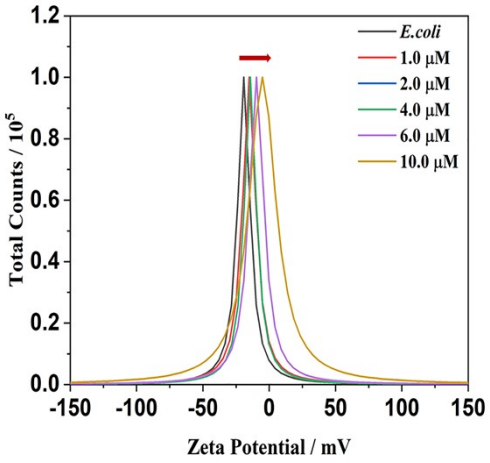

Fig. S25 Zeta-potentials of *E. coli* with different concertation (0-10 μM) of ***m*-TPEWP5⊃MC-G-NiB** (**NP2**) nanoparticles after 3rd irradiation cycles in phosphate-buffered solution.

20. SEM image

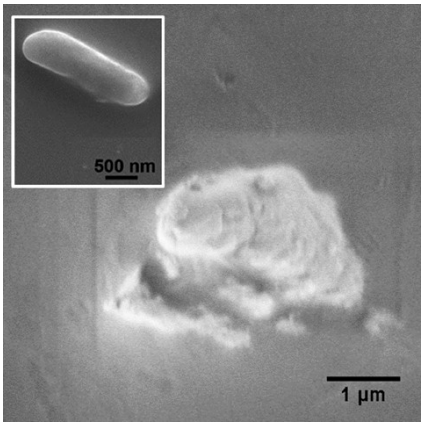

Fig. S26 SEM image of *E. coli* treated before (inset photo) and after incubating with ***m*-TPEWP5⊃MC-G-NiB** (**NP2**) nanoparticles (10 μM) after 3rd irradiation cycles.

21. References

S1. H. Wang, P. Zhang, B. P. Krishnan, M. Yu, J. Liu, M. Xue, S. Chen, R. Zeng, J. Cui, J. Chen, Switchable single fluorescent polymeric nanoparticles for stable white-light generation. *J. Mater. Chem. C* **2018**, *6*, 9897.

S2. E. J. Hong, P. Sivakumar, V. Ravichandran, D. G. Choi, Y. S. Kim, M. S. Shim, Pro-oxidant drug-loaded Au/ZnO hybrid nanoparticles for cancer-specific chemo-photodynamic combination therapy. *ACS Biomater. Sci. Eng.* **2019**, *5*, 5209.

S3. J. Ji, X. Li, T. Wu, F. Feng, Spiropyran in nanoassemblies as a photosensitizer for photoswitchable ROS generation in living cells. *Chem. Sci*. **2018**, *9*, 5816.

S4. Y. Yang, H. Hu, L. Chen, H. Bai, S. Wang, J.-F. Xu, X. Zhang, Antibacterial supramolecular polymers constructed via self-sorting: promoting antibacterial performance and controllable degradation. *Mater. Chem. Front.* **2019**, *3*, 806.

S5. X. Tian, M. Zuo, P. Niu, K. Velmurugan, K. Wang, Y. Zhao, L. Wang, X.-Y. Hu, Orthogonal design of a water-Soluble meso-tetraphenylethene-functionalized pillar[5]arene with aggregation-induced emission property and its therapeutic application. *ACS Appl. Mater. Interfaces* **2021**, *13*, 37466.

S6. F. C. Ho, Y. J. Huang, C. C. Weng, C. H. Wu, Y. K. Li, J. I. Wu, H. C. Lin, Efficient FRET approaches toward copper(II) and cyanide detections via host–guest interactions of photo-switchable [2]pseudo-rotaxane polymers containing naphthalimide and merocyanine moieties. *ACS Appl. Mater. Interfaces* **2020**, *12*, 53257.

S7. J.-J. Li, H.-Y. Zhang, G. Liu, X. Dai, L. Chen, Y. Liu, Photocontrolled light-harvesting supramolecular assembly based on aggregation-induced excimer emission. *Adv. Optical Mater.* **2021**, *9*, 2001702.

S8. E. Zhao, Y. Chen, H. Wang, S. Chen, J. W. Lam, C. W. Leung, Y. Hong, B. Z. Tang, Light-enhanced bacterial killing and wash-free imaging based on AIE fluorogen. *ACS Appl. Mater. Interfaces* **2015**, *7*, 7180.